Insights into the effect of inner polarization and multiple Ag-O units on high-efficient Ag-based photocatalyst

Mengmeng Li, Ying Dai*, Xiangchao Ma, Tao Jing, Baibiao Huang

School of Physics, State Key Laboratory of Crystal Materials, Shandong University, Jinan 250100, People's Republic of China

ABSTRACT

Ag-based materials are one kind of important photocatalysts. In the present work, the electronic structure and related properties of $Ag_6Si_2O_7$, Ag_2O and Ag_3PO_4 are systematically investigated by first principle calculations. The origin of the high photocatalytic activity of $Ag_6Si_2O_7$ is analyzed. Our results indicate that compared with Ag_2O and Ag_3PO_4, the multiple Ag-O units in $Ag_6Si_2O_7$ result in the separate distribution of holes and electrons, which are driven by the built-in electric field to transfer in different regions, contributing to the high photocatalytic activity by reducing the recombination of carriers. The intrinsic transfer of carriers tends to along [010] direction, leading to the best photocatalytic activity of the polar (010) surface though the high cleavage energy limits its exposure to some extent. In addition, the most possible exposed (100) surface corresponding to the lowest surface energy, with holes trapped at surface layers and electrons flowing into bulk region, is also advantageous to the photo-oxidation reaction. Therefore compared with other Ag-based photocatalytic materials, $Ag_6Si_2O_7$ shows the main advantages in the transfer and separation of carriers, and its high photocatalytic activity can be understood well. We expect this work can be helpful to guide the exploration of new photocatalysts with higher photocatalytic activity.

© 2016 Elsevier B.V. All rights reserved.

1. Introduction

As a promising strategy to cope with environmental pollution and energy shortage, photocatalysis has attracted much attention. However, the practical application of photocatalyst limited by the low efficiency is still some way off. For this purpose, extensive researches have been carried out to develop efficient photocatalytic materials in both experiment and theory. Besides modifying the traditional photocatalytic materials, such as TiO_2 and ZnO to overcome the detrimental factors of photocatalysis [1–6], developing new photocatalytic materials with some intrinsic and unique properties is also an important way [7–11]. Among them, Ag-based materials are one kind of important photocatalysts [10–17]. Both the plasmonic photocatalysts such as Ag@AgX (X = Cl, Br, I) [12–14] and Ag-based composite oxide photocatalysts such as Ag_3PO_4 [10], $AgAlO_2$ [15], $Ag_2Nb_4O_{11}$ [16] and $AgNbO_3$ [17] show fine photocatalytic performance. Particularly, Ag_3PO_4 was observed to show pretty high photocatalytic activity for photodegradation of organic dye and photooxidation water for O_2 generation with the visible light response [10].

Nevertheless, in recent experiment, Lou et al. synthesized $Ag_6Si_2O_7$ showed higher photodegradation rate of MB than Ag_3PO_4 and Ag_2O [11]. Though the internal polar electric field and the nonequivalent metal-oxygen polyhedra were analyzed to promote the transfer of carries then benefit the photocatalytic activity of $Ag_6Si_2O_7$, their action mechanism for the high photocatalytic activity is still not clear, but of great importance to understand the photocatalytic process and further improve the photocatalytic efficiency. Therefore in the present work, we comparatively study the intrinsic transfer and separation ability of electrons and holes in Ag_2O, Ag_3PO_4 and $Ag_6Si_2O_7$ systems from the effective masses, and the effect of different coordinated Ag atoms and the built-in electric field on the photocatalytic activity of $Ag_6Si_2O_7$ in details. Meanwhile given that the actual exposure of the surfaces is directly related to the photocatalytic performance, the surfaces are further discussed to examine other possible factors of the high photocatalytic activity for $Ag_6Si_2O_7$. Our results show compared with Ag_2O and Ag_3PO_4, the larger difference between the effective masses of holes and electrons in $Ag_6Si_2O_7$ is beneficial to the separation of carriers. Furthermore, the separated distribution of holes and elec-

---
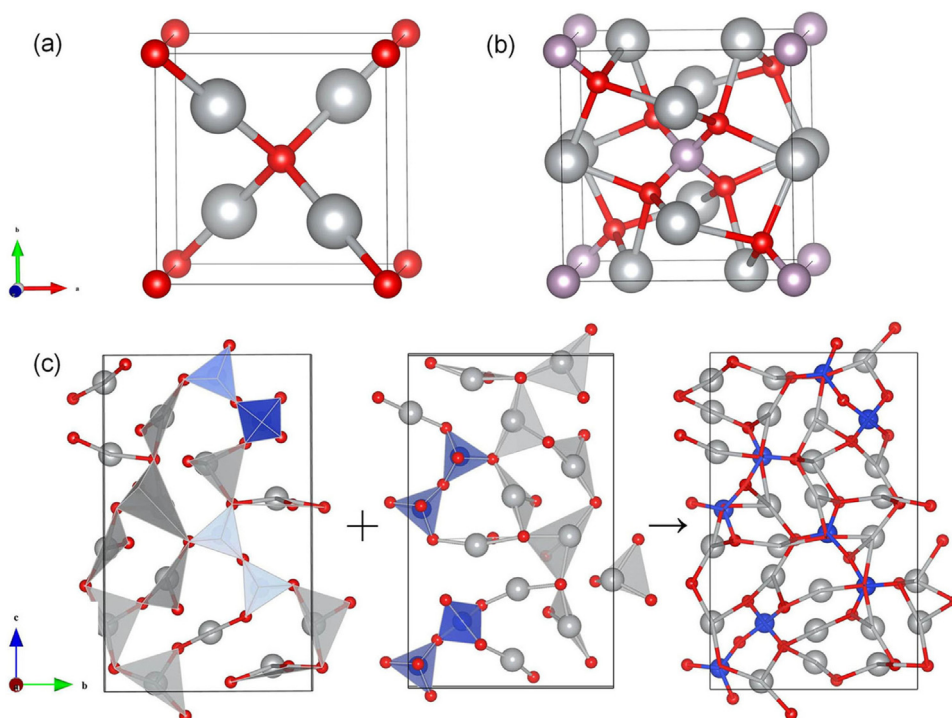
Fig. 1. The crystal structure of Ag_2O (a), Ag_3PO_4 (b) and $Ag_6Si_2O_7$ (c) constructed by stacking two same layers along [100] direction. Red, gray, mauve and blue balls denote O, Ag, P and Si atoms, respectively. (For interpretation of the references to colour in this figure legend, the reader is referred to the web version of this article.)

trons due to the existence of different coordinated Ag atoms, as well as the electric dipole moments results in more effective transfer and separation of carriers, then contributes to the high photocatalytic activity of $Ag_6Si_2O_7$, especially the (010) surface in which the carriers tend to accumulate. Whereas the high cleave energy of the polar surface limits its main exposure. Therefore the most stable (100) surface, expected as the main exposed surface is also discussed to analyze the efficient photocatalytic activity of $Ag_6Si_2O_7$. Our results show that both the trapped holes at (100) surface and the spatial separation of electrons and holes are beneficial to the photocatalytic activity of $Ag_6Si_2O_7$. This investigation can provide a deep insight for the effect of inner polarization and multiple Ag-O units on the high photocatalytic activity of $Ag_6Si_2O_7$ and guide the design and development of other high-efficient photocatalysts.

2. Computational methods

Our first principle calculations were performed using Vienna Ab-initio Simulation Package (VASP) code [18]. Both the bulk and surface models of $Ag_6Si_2O_7$ were used in this work. Five stoichiometric slab models were constructed to represent the (100), (010) and (001) surfaces of $Ag_6Si_2O_7$ with every slab model including 5 fold unit cells and 300 atoms, which were proved enough for the convergence of surface energy. 20 Å thick vacuum layer was used to avoid the interaction between the adjacent layers. The projector-augmented wave (PAW) was used to describe the electron-ion interaction [19]. In the calculations of surface models and structure optimization of bulk, the exchange correction energy adopted generated gradient approximation (GGA) with the form of Perdew-Burke-Ernzerhof (PBE) [20]. In addition, the Heyd-Scuseria-Ernzerhof (HSE06) hybrid functional which was proved to give a good description for electronic properties was used to the electronic structure calculation for the bulk models [21,22]. The 25%, 33% and 25% Hartree-Fock exchange were added to the PBE functional for Ag_2O [23], Ag_3PO_4 [24,25] and $Ag_6Si_2O_7$ [11], respectively. Both in bulk and surface calculations, the 400 eV cutoff
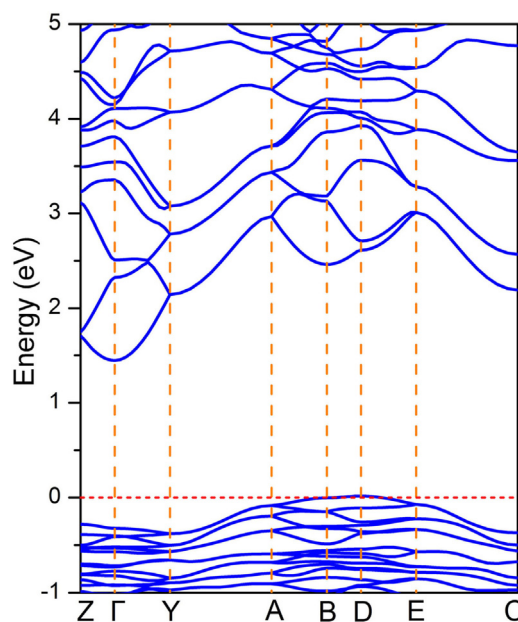

Fig. 2. The energy band of $Ag_6Si_2O_7$. Fermi level is set at 0 eV.

energy for the plane-wave basis set was adopted. Both the lattice constants and internal coordinates were relaxed for the bulk models, while the relaxation of the atoms was carried out based on the optimized bulk lattice parameters for surface models, with the convergence of force set as 0.02 eV/Å. The $7 \times 7 \times 7$, $5 \times 5 \times 5$ and $4 \times 2 \times 1$ k-point meshes were used to sample the Brillouin zone of Ag_2O, Ag_3PO_4 and $Ag_6Si_2O_7$, respectively. And the $3 \times 2 \times 1$, $2 \times 5 \times 1$ and $5 \times 3 \times 1$ k-point meshes were used for the (100), (010) and (001) surface of $Ag_6Si_2O_7$, respectively.
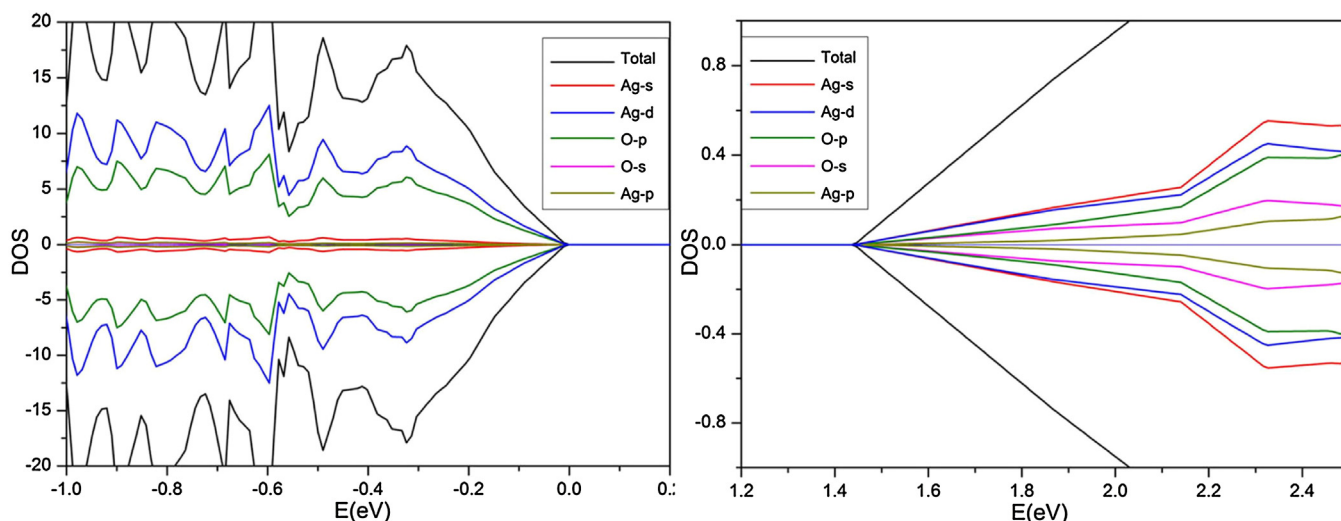
Fig. 3. The total and partial density of states of $Ag_6Si_2O_7$. The Fermi level is set at 0 eV. (For interpretation of the references to colour in this figure legend, the reader is referred to the web version of this article.)
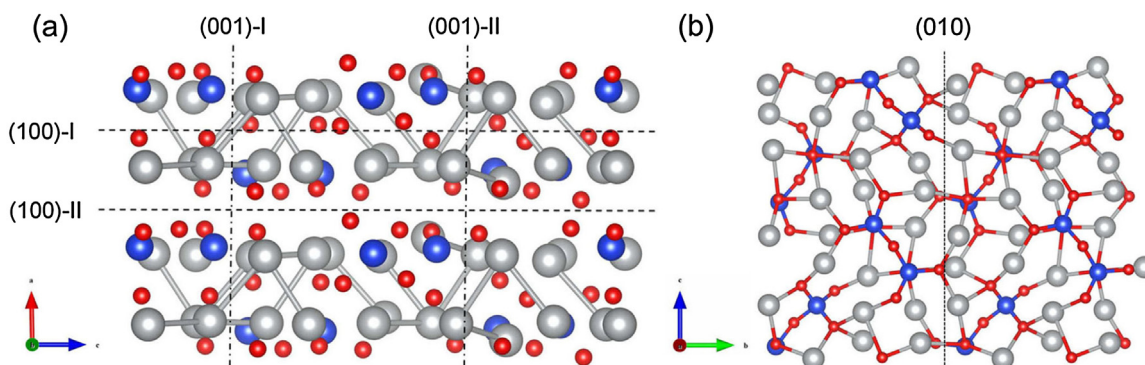
Fig. 4. The discontinuous d^{10}-d^{10} interaction (Ag—Ag bonds) along [100] direction and the different cleavage ways selected to construct the (100), (001) surface with different terminals (a); the cleavage position for the generation of (010) surface (b). (For interpretation of the references to colour in this figure legend, the reader is referred to the web version of this article.)

3. Results and discussions

3.1. Structure and electronic structure

As shown in Fig. 1, both Ag_2O and Ag_3PO_4 are cubic phase structure with two-coordinated and four-coordinated Ag atoms respectively, while the $Ag_6Si_2O_7$ belongs to monoclinic crystal system with P21 space group and possesses more complicated Ag-O coordination environment with three kinds of AgO units ([AgO_2], [AgO_3] and [AgO_4]). For convenience, the Ag atoms in [AgO_2], [AgO_3] and [AgO_4] units are labeled as Ag(a), Ag(b) and Ag(c), respectively. From the following analysis, we will see that the multiple Ag-O units in $Ag_6Si_2O_7$ result in the local layered distribution of holes instead of the homogeneous distribution in Ag_2O and Ag_3PO_4, which can contribute to the effective transfer and separation of carriers. On the other hand, the $Ag_6Si_2O_7$ is composed by two same layers alternately stacking along [100] direction with one of the layers rotating 180° and translating along [010] direction. Therefore a nonzero polar electric field is only found along [010] direction with the dipole moments along other directions offset due to the 180° rotation around [010] direction [11]. The inner polarization plays an important part in the photocatalytic process, which will be discussed in detail later.

In order to analyze the electronic properties and then the photocatalytic activity, the energy band structure of $Ag_6Si_2O_7$ is calculated firstly, with the result shown in Fig. 2. From the energy band, we can see that $Ag_6Si_2O_7$ is an indirect band gap semiconductor with the band gap of 1.44 eV, which is consistent with the previous experimental result of 1.58 eV [11], lower than the band gap of Ag_3PO_4 (2.45 eV) [10] and slightly higher than the band gap of Ag_2O (1.3 eV) [26]. The suitable band gap ensures its visible light response and high solar energy absorption. Meanwhile the indirect band gap with the conduction band minimum (CBM) at G and valence band maximum (VBM) at D, makes the recombination of photogenerated electrons and holes confined, considering that the interaction with phonon is further needed to satisfy the momentum conservation, which is also favorable to the photocatalytic activity. More information about the transfer of electrons and holes can be obtained by analyzing band edge dispersion. The more dispersive the band edge is, the faster transfer the carriers can achieve. It can be seen that the CBM is more dispersive than VBM, indicating the easier transfer of electrons than holes. Moreover, the dispersion of the band edge is also different along different directions, so the anisotropic effective masses are expected.

3.2. Anisotropic transfer of carriers characterized by effective mass

Furthermore, the effective masses of electrons and holes along three typical directions ([100], [010] and [001] direction) are calcu-
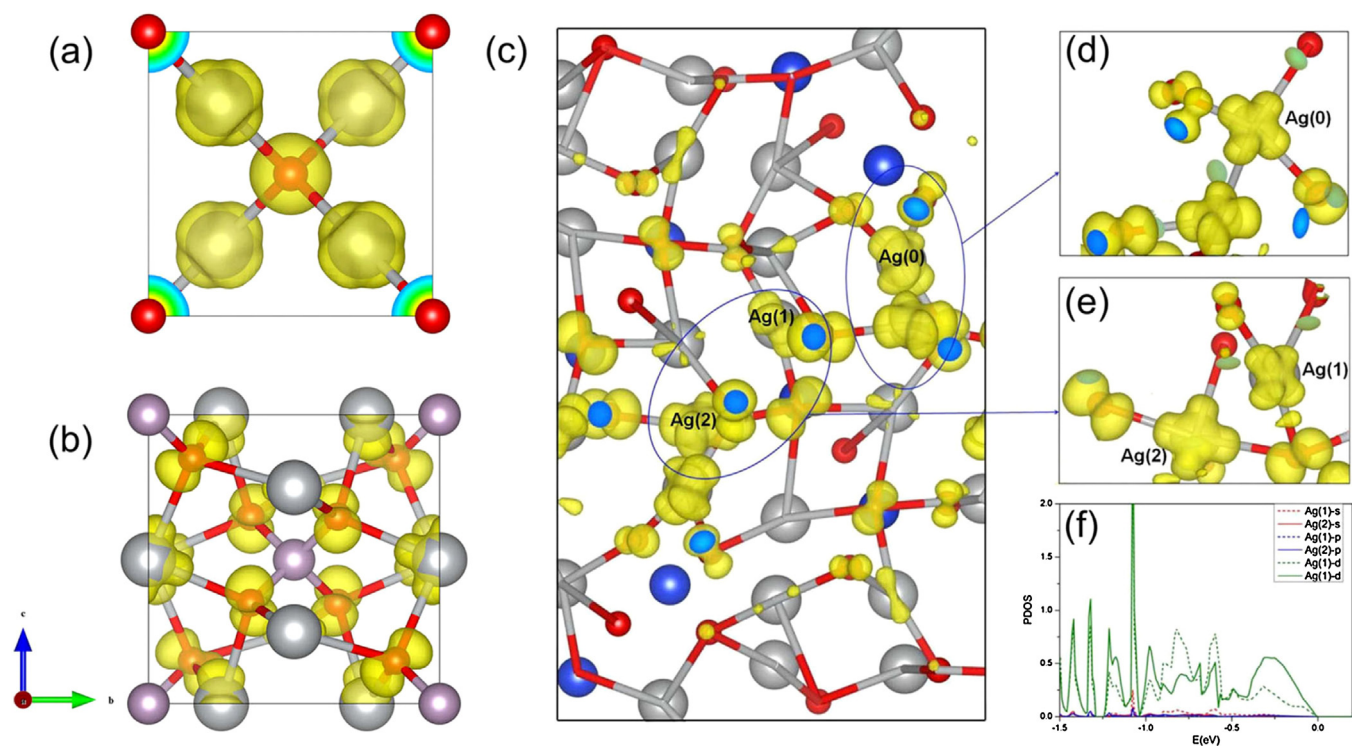
Fig. 5. (a)–(c) are the partial charge density around VBM of Ag_2O, Ag_3PO4 and $Ag_6Si_2O_7$, respectively. (d) and (e) are the enlarged views of the selected regions in (c). (f) corresponds to the PDOS of the two Ag atoms marked in (e). (For interpretation of the references to colour in this figure legend, the reader is referred to the web version of this article.)
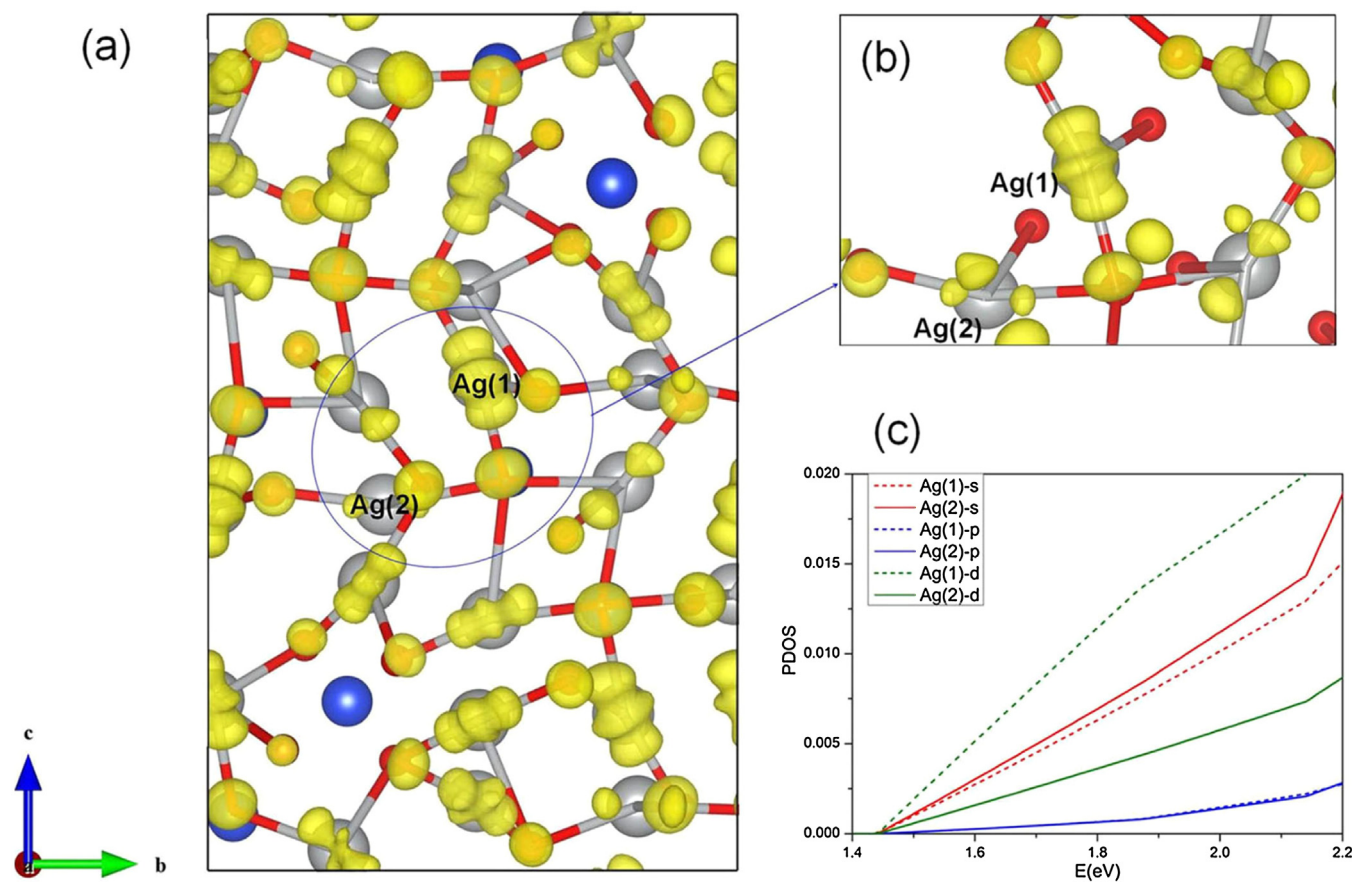
Fig. 6. (a) is the partial charge density around CBM in $Ag_6Si_2O_7$. (b) is the enlarged view of the selected region in (a). (c) corresponds to the PDOS of the two Ag atoms marked in (b). (For interpretation of the references to colour in this figure legend, the reader is referred to the web version of this article.)
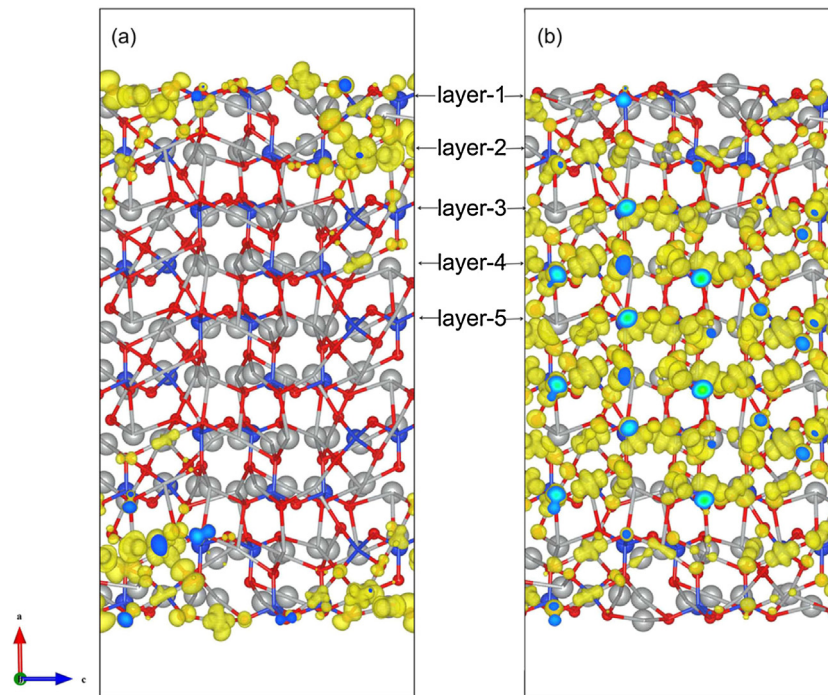
Fig. 7. The charge density distribution of the (100)-II surface at VBM (a) and CBM (b). (For interpretation of the references to colour in this figure legend, the reader is referred to the web version of this article.)
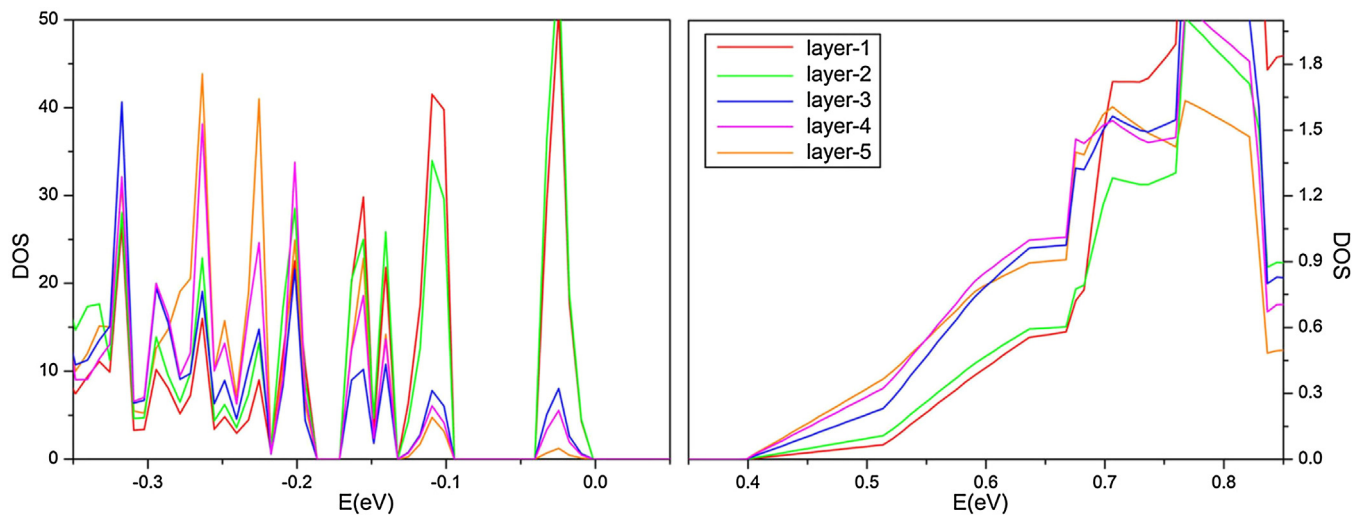
Fig. 8. The DOS of different layers in the (100)-II surface model with the layer-1 to layer-5 (from surface to inner). The marks of layers are shown in Fig. 7. The Fermi level is at 0 eV. (For interpretation of the references to colour in this figure legend, the reader is referred to the web version of this article.)

Table 1
Effective masses of electrons (m_e^*) and holes (m_h^*) along different directions in Ag_2O, Ag_3PO_4 and $Ag_6Si_2O_7$ in the unit of free-electron mass (m_e).

	Ag_2O		$Ag_6Si_2O_7$		Ag_3PO_4	
Direction	m_e^*	m_h^*	m_e^*	m_h^*	m_e^*	m_h^*
[100]	0.51	2.45	0.69	1.70 2.38[b]	0.42	1.62
	0.61(0.47)[a]	2.06(2.34)[a]			0.41(0.41)[a]	1.92(1.74)[a]
[010]	–	–	0.45	3.67	–	–
			0.53[b]			
[001]	–	–	0.50	3.48	–	1.00
						1.04(0.99)[a]

a Reference [27].
b Reference [30].

lated by fitting the parabolic functions to the CBM and VBM along different directions in the reciprocal space to discuss the intrin-

sic transfer ability of carriers in $Ag_6Si_2O_7$ [27,28]. For comparison, the effective masses of electrons and holes in Ag_2O and Ag_3PO_4

are also calculated, listed in Table 1. And some previous results are also given here as references including the results obtained by LDA and LAD + U calculations with the calculated values by LDA + U in bracket. From Table 1, we can see that our values of effective masses calculated by HSE is very close to the results obtained from the LDA + U calculation, which can further verify the reliability of our calculations. In $Ag_6Si_2O_7$, the electrons show the smaller effective masses than holes with the values of 0.45, 0.50 and 0.69 m_e along [010], [001] and [100] direction respectively. All of them are less than the effective masses of electrons in TiO_2 (about 1 m_e) [29], and close to the values in Ag_3PO_4 and Ag_2O system [27]. Therefore, the small effective masses of electrons in $Ag_6Si_2O_7$ resulting in the fast transfer of electrons are beneficial to the photocatalytic activity, but not the main reason for its higher photocatalytic efficiency than that of Ag_3PO_4 and Ag_2O as observed in experiment [11]. On the other hand, the effective masses of holes are pretty large in $Ag_6Si_2O_7$ with the values of 1.70, 3.67 and 3.48 m_e along [100], [010] and [001] direction, respectively. These results are consistent with the previous calculations in general [30]. The large difference between the effective masses of electrons and holes is conductive to the separation of them then can improve the photocatalytic activity. In this regard, the transfer and separation of carriers are easier in $Ag_6Si_2O_7$ than in Ag_2O and Ag_3PO_4. Furthermore, in $Ag_6Si_2O_7$, the optimal transfer direction of electrons and holes are [010] and [001] directions, given that electrons show the relative large and close effective masses with holes along [100] direction.

To analyze the origin of the different transfer ability of electrons and holes in $Ag_6Si_2O_7$, the density of states (DOS) and partial density of states (PDOS) are calculated. As shown in Fig. 3, the CBM of $Ag_6Si_2O_7$ mainly originates from the hybridization of Ag s and d states with the O p states, while the VBM is mainly composed of Ag d states and O p states with a little contribution from the Ag s states. Considering that the s states are more dispersive than p states, so the smaller effective masses of electrons due to the higher proportion of the contribution from s states to the CBM can be understood. It is worth mentioning that there are short Ag—Ag bonds (2.75–2.94 Å) in $Ag_6Si_2O_7$, close to the bonds length of 2.89 Å in metallic silver, which can be ascribed to the attractive interaction between Ag atoms, known as d^{10}-d^{10} interaction [31,32]. This Ag-Ag interactions provide the channels for the electrons transfer [33]. Nevertheless, unlike the continuously connected d^{10}-d^{10} interactions in other Ag-based semiconductors such as Ag_3PO_4, Ag_2SiO_3 [33], the d^{10}-d^{10} interactions of Ag atoms in $Ag_6Si_2O_7$ are discontinuous along [100] direction, as shown in Fig. 4(a), resulting in a relatively difficult transfer of electrons along this direction.

3.3. Preferred transfer of carriers promoted by built-in electric field

Though the transfer and separation of carriers along [010] and [001] directions are favored in $Ag_6Si_2O_7$ based on the suitable effective masses of electrons and holes, the real transfer is dependent on the specific coordination environment. Therefore the partial charge density around VBM and CBM (Figs. 5 and 6) are calculated to discuss the distribution of the excited electrons and holes as well as the transfer of them. Different from the delocalized distribution in Ag_2O (Fig. 5(a)) and Ag_3PO_4 (Fig. 5(b)), in $Ag_6Si_2O_7$, the VBM is mainly contributed by the middle region of the unit cell as shown in Fig. 5(c). The discontinuous layered-distribution along [001] direction limits the transfer of holes along this direction. Combining the analysis above, a preferred transfer of holes along [010] direction in $Ag_6Si_2O_7$ can be obtained. Meanwhile, the intrinsic built-in electric field further makes this transfer more effective.

Next, we pay more our attention to the transfer and separation of electrons and holes along [010] direction in $Ag_6Si_2O_7$. As shown in Fig. 5(c), the existence of the nonequivalent Ag-O units

and their inhomogeneous distribution give rise to the local distribution of holes, which mainly concentrate on the $[AgO_3]$ units between two $[AgO_4]$ units, including the central Ag(b) atoms and the O atoms linking Ag(b) and Ag(c). And we can see that most of atoms contributing to the VBM linked each other, constituting two chains along [010] direction, except the Ag(0) and Ag(1) atom as marked in Fig. 5(c). Though the two Ag atoms don't belong to the chains directly, both of them can be linked to the chains by Ag—O bonds or the direct Ag—Ag bonds. The enlarged Fig. 5(d) and (e) show these bonds clearly. As shown in Fig. 5(d), the Ag(0) atom and the Ag atom in the chain are bonded directly, then the exchange and transfer of holes between them can be achieved easily. Fig. 5(e) shows that Ag(1) atom and Ag(2) atom in the chain are linked by O atom. Fig. 5(f) further compares their PDOS at VBM, and the lager contribution from Ag(2) atom to VBM indicates an easy transfer of holes from Ag(1) to Ag(2) atom by the intermediate O atom. Therefore, the holes mainly concentrate in the chains in the middle region of unit cell, and there is a large portion of the wave function distribution along the Ag—O bonds in the chains, which can be served as the transfer channels of holes. Considering that the existence of the built-in electric field along same direction, the effective transfer of holes along these chains can be achieved. On the other hand, the states at CBM distribute more delocalized, almost spreading across the whole cell, as shown in Fig. 6(a). However, in the chains along which holes tend to transfer, the electrons distribute less (Fig. 6(b)). And the PDOS of Ag(1) and Ag(2) at CBM indicates that electrons tend to transfer from Ag(2) to Ag(1), away from the chains, due to the smaller contribution of Ag(2) atom to CBM. The spatial separation of the electrons and holes distribution reduces their recombination. And the effective transfer of holes along [010] direction driven by the built-in electric field can be achieved, which contributes to the higher photocatalytic activity of $Ag_6Si_2O_7$. Through the analysis above, we can see that $Ag_6Si_2O_7$ showed the main advantages than Ag_2O and Ag_3PO_4 in the transfer and separation of electrons and holes due to the presence of the inhomogeneous distribution of the multiple Ag-O units and the built-in electric field, which contribute to its high photocatalytic activity, especially the (010) surface because of the favorable transfer of carriers along [010] direction.

3.4. Surface exposure and related electronic properties

Although the (010) surface is placed high hopes, its exposure in samples is not preferred considering that the polar surface usually corresponds to the high surface energy [34,35], which is also verified by the following energy calculations. Therefore in the following, we concentrate on the discussion about the surface exposure and the corresponding photocatalytic activity. Three representative surfaces ((100), (010) and (001) surface) are investigated to analyze the surface properties. It is worth noting that there are two different cleavage ways to produce the symmetric and stoichiometric surface with different surface terminals for both (100) and (001) surfaces. The different cleavage ways are shown in Fig. 4(a) and the corresponding surfaces are referred to as the (100)-I, (100)-II, (001)-I and (001)-II surface, respectively. For the polar (010) surface, a proper cleavage way with the least bonds broken is used, as shown in Fig. 4(b). To determine the relative stability of these surfaces, the cleavage energy (E_{cl}) are calculated by the following equation:

$$E_{cl} = [E_{slab} - nE_{bulk}]/2S$$

Where E_{slab} and E_{bulk} are the total energy of slab and single $Ag_6Si_2O_7$, respectively, and n equals to the number of $Ag_6Si_2O_7$ in slab model. For symmetrical surface, the cleavage energy equals to the surface energy. The calculated cleavage energy of different

Table 2
The cleavage energy calculated for the different surfaces.

Surface	(100)		(001)		(010)
	I	II	I	II	
Cleavage energy (J/m^2)	0.87	0.10	0.49	0.77	0.71

surfaces are listed in Table 2. It can be seen that (100)-II surface shows the lowest cleavage energy, $0.10 J/m^2$, indicating that it is the most stable surface among the five surfaces. Compared with the energy of (100)-I surface, the lower surface energy of (100)-II surface may be attributed to the less Ag—Ag bonds needed to be broken. And the polar (010) surface does show relatively large cleavage energy indicating a weak stability then a restricted surface exposure. Consequently, we further study the properties of the (100) surface with the most stable configuration and analyze the corresponding photocatalytic activity.

In order to analyze the photocatalytic ability of (100)-II surface, the corresponding partial charge density at VBM and CBM are calculated firstly, with the results shown in Fig. 7. From the charge distribution, it can be seen that the charges contributing to the VBM and CBM are mainly localized at the first two layers and the inner layers, respectively, indicating that the holes are mainly trapped at the surface, while electrons distribute in bulk region mostly. The spatial separation of electrons and holes reduces their recombination. Meanwhile, considering that the low conduction band edge in $Ag_6Si_2O_7$ like in other Ag-based silicates $Ag_{10}Si_4O_{13}$ [36] and $Ag_9(SiO_4)_2NO_3$ [37], makes the excited electrons lack of enough reductive power, photo-oxidation reaction of holes mainly contribute to the experimental photodegradation. Therefore, the trapped surface holes can easily participate in the oxidation reaction with the surface adsorbates directly, avoiding the recombination of electrons and holes in the transfer process of holes from inside to surface, then improving the photocatalytic activity.

In addition, the corresponding calculated DOS shown in Fig. 8 further confirm the distribution and transfer of holes and electrons. It is shown that for layer 1–5 from top to inner (shown in Fig. 7), both the position of the highest occupied states and the lowest unoccupied states are unchanged, while the band edge contribution from the different layers varies. The first two layers show almost the same contribution to the VBM, and from layer 3 to layer 5, the contribution becomes less and less. It indicates there is an energy gradient driving holes from inner to surface, interpreting the trapping of holes at surface. However, compared with the contribution to VBM, the distribution of the states of different layers at CBM shows the opposite trend with an increasing distribution from surface to inner layers. So that, the transfer of electrons from surface to inner is expected for the existence of such energy gradient. These results further explain the different distribution of holes and electrons and the advantageous photooxidation activity of the (100) surface.

4. Conclusions

The structure and electronic related properties of $Ag_6Si_2O_7$, Ag_2O and Ag_3PO_4 are researched to understand the high photocatalytic activity of Ag-based material $Ag_6Si_2O_7$ based on first principle calculations in details. The transfer of carriers and the surface exposure investigation reveal that the pretty large difference of the transfer ability and uninterrupted distribution of electrons and holes as well as the continuously connected Ag—Ag bonds result in the preferred transfer and separation of carriers along [010] direction. Compared with Ag_2O and Ag_3PO_4, the unique structure of $Ag_6Si_2O_7$ give rise to the built-in electric field and the separate distribution of electrons and holes. The layered distribution

of holes are driven by built-in electric field to transfer along [010] direction with less recombination with electrons due to the different spatial distribution, contributing to the higher photocatalytic activity, especially making the (010) surface with obvious advantages for photocatalytic reaction even though the limited exposure due to the relative high cleave energy of the polar surface. On the other hand, the relative low surface energy of (100) surface makes its easy exposure. The existence of the opposite energy gradient for electrons and holes from inner to surface, resulting in the surface trapping of holes and the inner distribution of electrons which is beneficial to the direct photooxidation activity at the exposed (100) surface. So that, there is expressly advantages in the transfer and separation of carriers for $Ag_6Si_2O_7$ compared with other Ag-based photocatalytic materials. We expect this work can help to understand and further improve the photocatalytic performance for $Ag_6Si_2O_7$, and to inspire the development and designing of other efficient photocatalysts.

References

[1] R. Asahi, T. Morikawa, T. Ohwaki, K. Aoki, Y. Taga, Visible-light photocatalysis in nitrogen-doped titanium oxides, Science 293 (2001) 269–271.

[2] Y. Ma, X.L. Wang, Y.S. Jia, X.B. Chen, H.X. Han, C. Li, Titanium dioxide-based nanomaterials for photocatalytic fuel generations, Chem. Rev. 114 (2014) 9987–10043.

[3] R. Georgekutty, M.K. Seery, S.C. Pillai, A highly efficient Ag-ZnO photocatalyst: synthesis, properties, and mechanism, J.Phys. Chem. C 112 (2008) 13561–13563.

[4] J.P. Wang, Z.Y. Wang, B.B. Huang, Y.D. Ma, Y.Y. Liu, X.Y. Qin, X.Y. Zhang, Y. Dai, Oxygen vacancy induced band-gap narrowing and enhanced visible light photocatalytic activity of ZnO, ACS Appl. Mater. Interfaces 4 (2012) 4024–4030.

[5] J. Wang, Y. Xia, Y. Dong, R.S. Chen, L. Xiang, S. Komarneni, Defect-rich ZnO nanosheets of high surface area as an efficient visible-light photocatalyst, Appl. Catal. B: Environ. 192 (2016) 8–16.

[6] Y.J. Wang, R. Shi, J. Lin, Y.F. Zhu, Enhancement of photocurrent and photocatalytic activity of ZnO hybridized with graphite-like C_3N_4, Energy Environ. Sci. 4 (2011) 2922–2929.

[7] G. Wang, B.B. Huang, X.C. Ma, Z.Y. Wang, X.Y. Qin, X.Y. Zhang, Y. Dai, M.H. Whangbo, $Cu_2(OH)PO_4$, a near-infrared-activated photocatalyst, Angew. Chem. Int. Ed. 52 (2013) 4810–4813.

[8] X.C. Wang, K. Maeda, A. Thomas, K. Takanabe, G. Xin, J.M. Carlsson, K. Domen, M. Antonietti, A metal-free polymeric photocatalyst for hydrogen production from water under visible light, Nat. Mater. 8 (2009) 76–80.

[9] L.Q. Ye, Y.R. Su, X.L. Jin, H.Q. Xie, C. Zhang, Recent advances in BiOX (X = Cl, Br and I) photocatalysts: synthesis, modification, facet effects and mechanisms, Environ. Sci.: Nano 1 (2014) 90–112.

[10] Z.G. Yi, J.H. Ye, N. Kikugawa, T. Kako, S.X. Ouyang, H.S. Williams, H. Yang, J.Y. Cao, W.J. Luo, Z.S. Li, Y. Liu, R.L. Withers, An orthophosphate semiconductor with photooxidation properties under visible-light irradiation, Nat. Mater. 9 (2010) 559–564.

[11] Z.Z. Lou, B.B. Huang, Z.Y. Wang, X.C. Ma, R. Zhang, X.Y. Zhang, X.Y. Qin, Y. Dai, M.H. Whangbo, $Ag_6Si_2O_7$: a silicate photocatalyst for the visible region, Chem. Mater. 26 (2014) 3873–3875.

[12] P. Wang, B.B. Huang, X.Y. Qin, X.Y. Zhang, Y. Dai, J.Y. Wei, M.H. Whangbo, Ag@AgCl: a highly efficient and stable photocatalyst active under visible light, Angew. Chem. Int. Ed. 47 (2008) 7931–7933.

[13] M.S. Zhu, P.L. Chen, M.H. Liu, Graphene oxide enwrapped Ag/AgX (X = Br, Cl) nanocomposite as a highly efficient visible-light plasmonic photocatalyst, ACS Nano 5 (2011) 4529–4536.

[14] X.C. Ma, Y. Dai, L. Yu, B.B. Huang, Energy transfer in plasmonic photocatalytic composites, Light: Sci. Appl. 5 (2016) e16017.

[15] S.X. Ouyang, H.T. Zhang, D.F. Li, T. Yu, J.H. Ye, Z.G. Zou, Electronic structure and photocatalytic characterization of a novel photocatalyst $AgAlO_2$, J. Phys. Chem. B 110 (2006) 11677–11682.

[16] H.J. Dong, G. Chen, J.X. Sun, Y.J. Feng, C.M. Li, C.D. Lv, Stability, durability and regeneration ability of a novel Ag-based photocatalyst, $Ag_2Nb_4O_{11}$, Chem. Commun. 50 (2014) 6596–6599.

[17] H. Kato, H. Kobayashi, A. Kudo, Role of Ag^+ in the band structures and photocatalytic properties of $AgMO_3$ (M: Ta and Nb) with the perovskite structure, J. Phys. Chem. B 106 (2002) 12441–12447.

[18] G. Kresse, J. Furthmüller, Efficiency of ab-initio total energy calculations for metals and semiconductors using a plane-wave basis set, Comput. Mater. Sci. 6 (1996) 15–50.

[19] P.E. Blöchl, Projector augmented-wave method, Phys. Rev. B 50 (1994) 17953–17979.

[20] J.P. Perdew, K. Burke, M. Ernzerhof, Generalized gradient approximation made simple, Phys. Rev. Lett. 77 (1996) 3865–3868.

[21] J. Heyd, G.E. Scuseria, M. Ernzerhof, Hybrid functionals based on a screened coulomb potential, J. Chem. Phys. 118 (2003) 8207–8215.

[22] J. Heyd, G.E. Scuseria, M. Ernzerhof, Erratum: Hybrid functionals based on a screened Coulomb potential, J. Chem. Phys. 124 (2003) 219906.

[23] J.P. Allen, D.O. Scanlon, G.W. Watson, Electronic structures of silver oxides, Phys. Rev. B 84 (2011) 115141.

[24] P. Reunchan, N. Umezawa, Sulfur and silicon doping in Ag_3PO_4, J. Phys. Chem. C 119 (2015) 2284–2289.

[25] Y. Huang, T. Ma, Q.Y. Chen, C. Cao, Y. He, The electronic properties of impurities (N, C, F, Cl, and S) in Ag_3PO_4: a hybrid functional method study, Sci. Rep. 5 (2015) 12750.

[26] L.H. Tjeng, M.B.J. Meinders, J. van Elp, J. Ghijsen, G.A. Sawatzky, R.L. Johnson, Electronic structure of Ag_2O, Phys. Rev. B 41 (1990) 3190–3199.

[27] N. Umezawa, S.X. Ouyang, J.H. Ye, Theoretical study of high photocatalytic performance of Ag_3PO_4, Phys. Rev. B 83 (2011) 035202.

[28] X. Ma, Y. Dai, M. Guo, B. Huang, The role of effective mass of carrier in the photocatalytic behavior of silver halide-based Ag@AgX (X = Cl, Br, I): a theoretical study, ChemPhysChem 13 (2012) 2304–2309.

[29] D. Kurita, S. Ohta, K. Sugiura, H. Ohta, K. Koumoto, Carrier generation and transport properties of heavily Nb-doped anatase TiO_2 epitaxial films at high temperatures, J. Appl. Phys. 100 (2006) 096105.

[30] Y. Obukuro, K. Ninomiya, S. Matsushima, H. Nakamura, K. Obata, G. Sakai, M. Arai, K. Kobayashi, Electronic structure of photoresponsive $Ag_6M_2O_7$ (M = Si, Ge), J. Ceram. Soc. Jpn. 124 (2016) 116–121.

[31] M. Jansen, Homoatomic d-d" interactions: their effects on structure and chemical and physical properties, Angew. Chem. Int. Ed. Engl. 26 (1987) 1098–1110.

[32] P. Mehrotra, R. Hoffmann, Cu(1)-Cu(1) interactions. bonding relationships in d^{10}-d^{10} systems, Inorg. Chem. 17 (1978) 2187–2189.

[33] T.G. Kim, D.H. Yeon, T. Kim, J. Lee, S.J. Im, Silver silicates with three-dimensional d^{10} −d^{10} interactions as visible light active photocatalysts for water oxidation, Appl. Phys. Lett. 103 (2013) 043904.

[34] J. Neugebauer, T. Zywietz, M. Scheffler, J.E. Northrup, C.G. Van de Walle, Clean and as-covered zinc-blende GaN (001) surfaces: novel surface structures and surfactant behavior, Phys. Rev. Lett. 80 (1998) 3097–3100.

[35] B. Meyer, D. Marx, Density-functional study of the structure and stability of ZnO surfaces, Phys. Rev. B 67 (2003) 035403.

[36] X.L. Zhu, P. Wang, B.B. Huang, X.C. Ma, X.Y. Qin, X.Y. Zhang, Y. Dai, Synthesis of novel visible light response $Ag_{10}Si_4O_{13}$ photocatalyst, Appl. Catal. B: Environ. 199 (2016) 315–322.

[37] X.L. Zhu, Z.Y. Wang, B.B. Huang, W. Wei, Y. Dai, X.Y. Zhang, X.Y. Qin, Synthesis of $Ag_9(SiO_4)_2NO_3$ through a reactive flux method and its visible-light photocatalytic performances, APL Mater. 3 (2015) 104413.